NANO LETTERS

pubs.acs.org/NanoLett

Nonlinear Optical Response from Arrays of Au Bowtie Nanoantennas

Kaspar D. Ko,[†,§] Anil Kumar,[‡,§] Kin Hung Fung,[†] Raghu Ambekar,[‡] Gang Logan Liu,[‡] Nicholas X. Fang,[*,†] and Kimani C. Toussaint, Jr.[*,†,∥]

[†]Department of Mechanical Science and Engineering and [‡]Department of Electrical and Computer Engineering, University of Illinois at Urbana-Champaign, Urbana, Illinois 61801, United States

ABSTRACT We demonstrate that the optical response of a single Au bowtie nanoantenna can be favorably modified to increase the local intensity by a factor of 10^3 in the feed gap region when a periodic array of antennas are used. We find that the array periodicity can be used to modulate and shape the spectral emission. An analysis of the emission confirms the presence of second-harmonic generation and two-photon photoluminescence, typical of gold nanostructures, but also reveals a portion of the emitted spectrum that cannot be attributed to a single multiphoton process. Our investigations have important implications for understanding the role of resonant nanostructures in designing optical antennas for next-generation photonic technologies.

Recent investigations into the optical response of bowtie nanoantennas (BNAs) has established the tip-to-tip triangle configuration as promising for applications such as photonic circuits,[1] super-resolution imaging,[2] and single molecule detection.[3] BNAs have been shown to exhibit higher localized field enhancement and better spatial confinement of the applied electric field than other coupled-plasmon resonant-nanoparticle pair geometries.[4] The large E-field intensity enhancement arises from a combination of localized surface plasmon resonances in sharp tip geometries and an electrodynamic coupling between the two arms of the antenna, which leads to a confinement of the applied field in the subwavelength gap. This antenna effect also enhances nonlinear processes such as second-harmonic generation (SHG),[5] third harmonic generation (THG),[6] two-photon photoluminescence (TPPL),[7] and supercontinuum (SC) generation.[8]

The diverse set of useful optical properties of BNAs and the extent of control over them is well-known. Studies in the past few years have investigated the dependence of the field enhancement, field confinement, and optical resonances on various parameters of the geometry of the BNA including gap size,[4,6,7,9−12] antenna size,[4,6,9,10] and radius of curvature of the tip.[9,10] Furthermore, periodic arrays of nanostructures have recently been shown to exhibit near-field intensity enhancements 1 order of magnitude greater than those of an isolated nanostructure.[13,14] The large electric fields are also especially important for the nonlinear response[5,8,15−17] because of the polynomial dependence on the intensity. For BNAs, the electric field is confined to a subwavelength region in the feed gap separating the two arms. As a result, these properties allow the deliberate design of the BNA for a variety of applications. Here, we explore how the single BNA response can be considerably modulated by employing them in a periodic array and offer new information on how the nonlinear response is affected by the near-field intensity enhancements in our optical antenna system.

Using the dimensional tolerances of our fabrication technique as a guide, we simulated gold BNAs of 50 nm thickness and various sizes with a commercial FDTD software (from Lumerical Solutions, Inc.) to optimize the resonance behavior of single BNAs and their near-field intensity enhancement ($|E|^2/|E_{\text{incident}}|^2$) for our investigation. Because the BNA resonance is also strongly dependent on the polarization of the applied optical field, the measurements and simulations were performed using incident polarizations parallel and perpendicular to the bowtie axis, which we refer to as horizontal and vertical polarization, respectively. It was found that a single BNA composed of two equilateral triangles with 140 nm side lengths separated by a 20 nm gap (illustration in Figure 1a) shows a resonance peak near our laser wavelength of 780 nm for horizontal polarization (Figure 1c).

It has been previously shown that the resonance behavior of a gold nanospheroid can be dramatically modified when a periodic array of spheroids are used.[13,14,18] The dependence of the local field intensity as a function of spacing (or periodicity) can be understood from the coupled dipole equation.[14] The array-modified particle polarizability, α^*, depends on both the single particle polarizability, α, as well as a geometric arrangement parameter representing the influence of adjacent particles, S. Their relationship is given by $\alpha^* = 1/[(1/\alpha) - S]$. When the two terms in the denominator are comparable, the array-modified particle polarizability can be very large, thereby leading to significant intensity enhancement.[13,14,18]

* To whom correspondence should be addressed. E-mail: (N.X.F.) nicfang@illinois.edu; (K.C.T.) ktoussai@illinois.edu.

§ These authors contributed equally to this work.

∥ Affiliate in the Department of Electrical and Computer Engineering, and Bioengineering.

Received for review: 08/4/2010
Published on Web: 11/24/2010

DOI: 10.1021/nl102751m | *Nano Lett.* **2011,** *11,* 61–65

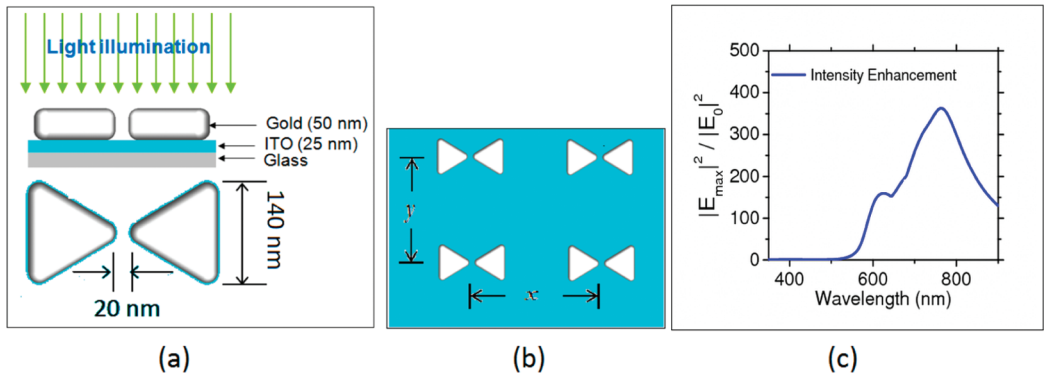

FIGURE 1. Bowtie nanoantennas. Illustration showing the dimensions of an individual bowtie nanoantenna on the substrate in (a) and showing the definition of the *x*- and *y*- center-to-center spacings in (b). Note that there is a 3 nm thick chromium adhesion layer (not shown) beneath the gold. FDTD simulation of the local electric-field intensity enhancement for an individual bowtie nanoantenna in (c).

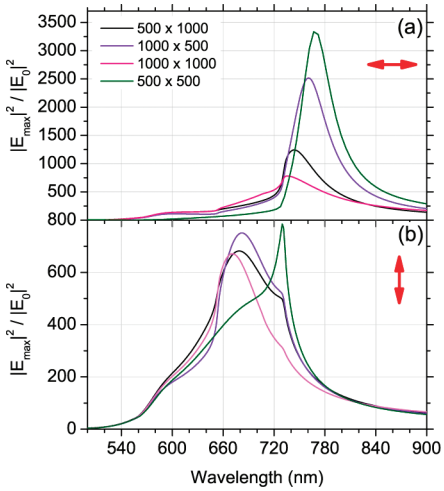

FIGURE 2. FDTD simulation of the local electric-field intensity enhancement 2 nm above the surface of the bowtie nanoantennas of various spacings for incident polarizations parallel (a) and perpendicular (b) to the main antenna axis, also indicated with red arrow.

We performed FDTD simulations with periodic boundary conditions for the optimized single BNAs having various in-plane spacings. The results in Figure 2 demonstrate the significant influence of a periodic array on the response, where strong near-field intensity enhancements for spacings of 500 nm are more than 10^3 times higher than that of the single BNA (Figure 1c). Since the single particle polarizability is kept constant in our design, the array-modified particle polarizability can be controlled through the array spacing. Furthermore, we found that selecting integer multiples of a particular spacing (the 500 nm spacing in our experiments) largely preserves the spectral position of the array resonance (inclination near wavelength of 730 nm in Figure 2b), while the strength of the near-field intensity is altered by the array-modified single BNA resonance, which is dependent on both polarization and spacing.

Using electron-beam lithography, we fabricated arrays of 50 nm thick gold BNAs with a 3 nm Cr adhesion layer onto a 50 nm thick ITO-coated quartz coverslip. The x (nm) and y (nm) center-to-center spacings (illustrated in Figure 1b) were 500 × 500, 500 × 1000, 1000 × 500, and 1000 × 1000, which each have varying degrees of near-field intensity enhancement, although the single BNA geometry in each array is identical. Each array was fabricated on the same coverslip in a 100 μm × 100 μm area and spaced 100 μm from each other. The arrays were illuminated using a Ti:sapphire laser (80 MHz repetition rate, 100 fs pulse width, center wavelength λ_{pump} = 780 nm) and brought to a focus on the sample in an inverted microscope (Olympus IX81) using a 100× (plan apochromat, numerical aperture of 1.4) oil-immersion objective. The nonlinear emission spectra were acquired in reflection geometry using the same objective, and coupled to a spectrometer (Jobin Yvon CP140−103 grating, Andor DU420A camera) using appropriate ancillary optics, including a 680 nm low-pass filter to reject the pump wavelengths. The spectrometer acquisition parameters were held constant and set to ensure high signal-to-noise ratio for the weakest signal. Prior to each measurement, the z-position of the objective was adjusted using an electron-multiplying charge-coupled device array detector (Hamamatsu C9100-3) and an autofocus program (IPLab 6.0), which uses a Gaussian contrast map to identify the z-position (or axial plane) that produces the highest contrast.

Several measures were also taken to minimize laser-induced structural damage due to the sensitivity of the optical properties of BNAs to their morphology. The excitation beam was stochastically scanned using a galvonometer-based scanner (dwell-time less than 150 μs) to achieve relatively uniform illumination.[19] This avoids the comparatively long dwell times and discrete sampling of beam positions associated with conventional raster scanning and permits the use of higher intensities while reducing the possibility of localized damage due to uneven sample coverage. The input data for the galvanometer-based scanner (Cambridge Technology) was produced at a rate of 7500 Hz using a pseudorandom white-noise generator (LabView). The total size of the scanned area was determined to be ~29 μm × 29 μm. For all measurements shown here, the average

DOI: 10.1021/nl102751m | *Nano Lett.* **2011,** *11,* 61–65

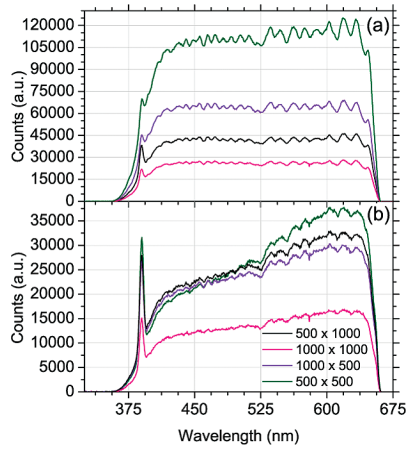

FIGURE 3. Nonlinear spectra of all array spacings for horizontal polarization (a) and for vertical polarization (b). Excitation wavelengths at 780 nm. Note that both *x*-axes have identical scales.

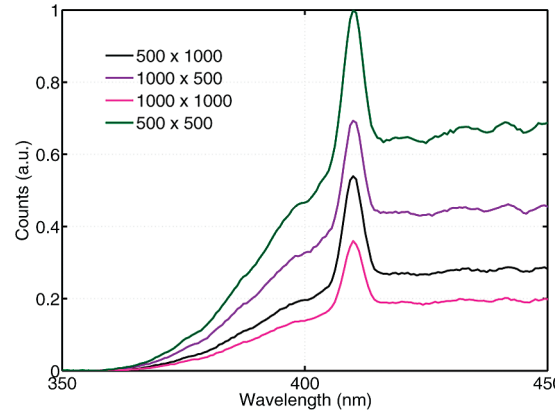

FIGURE 4. Nonlinear spectra of all array spacings for λ_{pump} = 820 nm zoomed in on SHG peak; 500 nm × 500 nm (green), 1000 nm × 500 nm (purple), 500 nm × 1000 nm (black), and 1000 nm × 1000 nm (pink), for horizontal polarization.

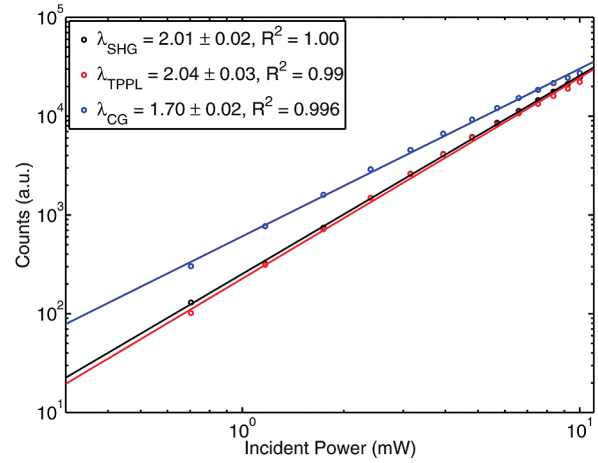

FIGURE 5. Power dependence test. Log−log plot of signal vs incident power of the 500 nm × 500 nm array for λ_{pump} = 780 nm and horizontal polarization. The mean values are shown as points with an ordinary least-squares fit shown as a line. The calculated slopes, 95% confidence intervals, and coefficients of determination are listed in the legend. Data points for statistical analysis are selected at three wavelengths in each spectral region on either side of the discontinuity at ≈525 nm (see Figure 3).

power was kept constant at 10 mW (peak power density ~10^{12} W/cm^2, peak fluence ~32 mJ/cm^2) and each measurement was collected from an unexposed area of the arrays with total exposure times (autofocus + acquisition) of less than 120 s. While other studies of similar coupled-dimer nanostructures typically involve intensities several orders of magnitude smaller than those used here,[4,6−8,16,20,20,21] we have experimentally determined our damage threshold to be 10 min at 25 mW (measured at the sample) by visual inspection of postirradiation SEM images of the BNAs. In addition, a test for optical damage at an average power of 10 mW exhibited remarkable signal stability for over an hour of irradiation.

The nonlinear emission spectra of the arrays of BNAs are shown in Figure 3. Each curve shows a narrowband emission at the second harmonic of the pump wavelength and a broadband continuum that extends to the limit of our detection window (~660 nm). An apparent discontinuity in the spectra is evident near the 525 nm wavelength as well as a slight curvature in the signal between the SHG peak and the discontinuity. The small fluctuations in the spectra occur at identical spectral locations for all arrays and incident polarizations. It is possibly due to a Fabry−Perot resonance between the sample and a protective coverslip (Corning No. 1) separating the sample from the oil-immersion objective. The peak at the second harmonic corresponds to SHG, which arises from a nonzero second-order nonlinear susceptibility due to symmetry-breaking at the gold−substrate and gold−air interfaces.[22] The SHG contribution from the gold−air interface is known to be amplified by large field enhancement in sharp gold tips.[23] The feed gap region of the BNA is analogous to the sharp tip and we find that arrays with higher near-field intensity enhancement are associated with higher SHG emission. This correlation with near-field intensity was also observed for the broadband continuum. However, the behavior of the continuum shown here is very different from those previously reported.[5,7,8,16]

The occurrence of a relatively constant emission over such a broad spectral range is unexpected for gold nanostructures. A power dependence test of signal versus incident power is shown in Figure 5 for 500 nm × 500 nm for λ_{pump} = 780 nm and horizontal incident polarization. An ordinary least-squares fit was performed at the SHG peak and for several wavelengths within each of the two regions of the emitted spectrum on either side of the discontinuity. This test yielded slopes (with 95% confidence intervals) of 2.01 ± 0.02, 2.04 ± 0.03, and 1.70 ± 0.02, respectively. The ~2 slope at the second-harmonic wavelength further confirms the emission as SHG. For the continuum region of the spectra, a slope of 2.04 suggests that the region between the SHG peak and the discontinuity is TPPL.[7,16] Interestingly, the continuum extends to the blue of the SHG peak, which is especially noticeable when λ_{pump} = 820 nm (Figure 4). Onuta et al. have reported that other mechanisms in addition to TPPL may be contributing to the continuum

DOI: 10.1021/nl102751m | *Nano Lett.* **2011,** *11,* 61–65

emission.[5] In fact, the power dependence for the region of the spectrum with wavelengths greater than 525 nm yields a slope of 1.70. This is in contrast to the emission reported by Mühlschlegel et al.[8] for gold rectangular dimers that was attributed to a four-photon nonlinear optical process that resulted in white-light supercontinuum generation from the ITO/glass substrate. They observed an emission occupying the same spectral region as TPPL that follows a fourth-order power dependence and vanishes completely for incident polarization perpendicular to the antenna axis. Here, we not only detect an appreciable signal over a broad region for vertical polarization (Figure 3b) but also do not observe a fourth-order dependence or a change in power dependence of the TPPL region over one decade of the power test. These results indicate that more complex nonlinear processes than those previously reported are responsible for the broadband continuum generation.

The underlying signal shape of each spectra in Figure 3 appears to be unique to the incident polarization. The horizontal polarization has a flat response to the red of the SHG peak, while the vertical polarization shows a sloping shape, which ultimately correspond to the efficiency of the mechanisms for TPPL and the rest of the continuum. Additionally, it was also observed (but not shown) that the spectral response for horizontal polarization at lower incident powers (<3 mW) has a sloping shape similar to the vertical polarizations. Polarization along the BNA axis promotes strong coupling of the two nanotriangles that comprise a single BNA and results in collective plasmon modes along the entire antenna,[12] suggesting that the shape of the continuum is due to a combination of polarization-dependent plasmon modes and incident power. Equally important, we see the spectral shapes of each of the arrays for a given polarization are similar (i.e., all are flat for horizontal, sloping for vertical) regardless of the strength of intensity enhancement. These unique dependencies point to nonlinear mechanisms that may be more sensitive to the individual particle, rather than the array.

Analyzing the relative emissions of the SHG and the continuum, using a nonlinear emission ratio, γ, as seen in Figure 6, can also provide insight to the origin of the nonlinear response. It is defined as $\gamma_{TPPL} = \lambda_{SHG}/\lambda_{463nm}$ and $\lambda_{635nm} = \lambda_{SHG}/\lambda_{635nm}$, where λ_{SHG}, λ_{463nm}, and λ_{635nm} are the signals at the wavelengths corresponding to the second harmonic, 463 and 635 nm, respectively. We choose this form for the ratio because of the direct relationship between experimental TPPL signal and simulated local intensity enhancement value derived by Schuck et al.[7] In addition, SHG is also known to be specifically related to field enhancement.[5,15,17,23] Thus, a given near-field intensity enhancement value (Figure 2) should be associated with both a TPPL signal and an SHG signal. However, comparing the values of γ_{TPPL}, the emission of SHG is proportionally higher than that of TPPL for vertical compared to horizontal polarization, where $\gamma_{TPPL} > 1$ in Figure 6a and $\gamma_{TPPL} < 1$ in Figure 6b.

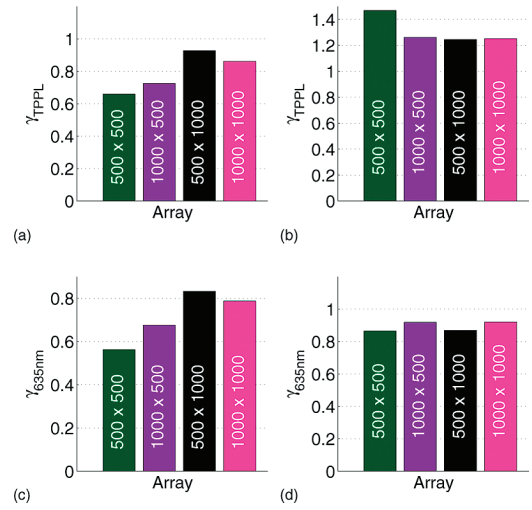

FIGURE 6. Nonlinear emission ratio calculated at 463 and 635 nm which are representative TPPL and the rest of the continuum, respectively. For $\lambda_{pump} = 780$ nm, and horizontal polarization, (a,c); for vertical polarization, (b,d). Array colors: 500 nm × 500 nm (green), 1000 nm × 500 nm (purple), 500 nm × 1000 nm (black), 1000 nm × 1000 nm (pink).

Combined with the occurrence of similar spectral shapes for each incident polarization (Figure 3), regardless of the array spacing (and therefore intensity enhancement), the nonlinear emission ratio indicates that the nonlinear mechanisms for one, or both, of SHG and TPPL are independent of the local intensity enhancement. When comparing γ_{TPPL} in Figure 6a to γ_{635nm} in Figure 6c, the magnitudes of γ show similar behavior relative to each array, but a comparison of Figure 6b and d do not show such similarities. A direct implication of these results is that a stronger local field does not neccessarily yield stronger SHG. The analysis of the nonlinear emission ratios for horizontal and vertical polarizations indicate that intensity enhancement may not be the limiting factor in enhancing SHG and other contributions may be more effective in boosting the SHG response.

In conclusion, through a series of FDTD simulations varying geometry and periodicity, we have shown that periodic arrays of BNAs can be successfully employed to further increase the large local intensity enhancements of single BNAs. As a result, we were able to use periodicity as an additional degree-of-freedom in manipulating the optical response and identified several characteristics of the nonlinear emission from arrays of BNAs. We observe SHG, TPPL, and a more complex photoluminescence that follows a power dependence of 1.70, but more importantly, resonantly excited arrays of BNAs were seen to exhibit a remarkably uniform emission over a spectral region of over 250 nm. It was found that higher intensity enhancement is associated with higher SHG and TPPL emission. However, our analysis suggests that high-intensity enhancements and resonance matching may not be the only preconditions for enhanced nonlinear emission. To our knowledge, this is the first report of implementing optical antennas in an array to favorably augment its optical response.

DOI: 10.1021/nl102751m | *Nano Lett.* **2011,** *11,* 61–65

Acknowledgment. This work was supported in part by funding from the ONR, the NSF, and the University of Illinois at Urbana-Champaign research start-up funds. We thank Santosh Tripatthi and Brian Roxworthy for a meticulous reading of this manuscript.

REFERENCES AND NOTES

(1) Bozhevolnyi, S.; Erland, J.; Leosson, K.; Skovgaard, P. *Phys. Rev. Lett.* **2001**, *86*, 3008–3011.
(2) Blaikie, R.; Melville, D. *J. Opt. A: Pure Appl. Opt.* **2005**, *7*, S176–S183.
(3) Kuhn, S.; Hakanson, U.; Rogobete, L.; Sandoghdar, V. *Phys. Rev. Lett.* **2006**, *97*, No. 017402.
(4) Fromm, D. P.; Sundaramurthy, A.; Schuck, P. J.; Kino, G.; Moerner, W. E. *Nano Lett.* **2004**, *4*, 957–961.
(5) Onuta, T. D.; Waegele, M.; DuFort, C. C.; Schaich, W. L.; Dragnea, B. *Nano Lett.* **2007**, *7*, 557–564.
(6) Hanke, T.; Krauss, G.; Trautlein, D.; Wild, B.; Bratschitsch, R.; Leitenstorfer, A. *Phys. Rev. Lett.* **2009**, 103.
(7) Schuck, P. J.; Fromm, D. P.; Sundaramurthy, A.; Kino, G. S.; Moerner, W. E. *Phys. Rev. Lett.* **2005**, 94.
(8) Mühlschlegel, P.; Eisler, H. J.; Martin, O. J. F.; Hecht, B.; Pohl, D. W. *Science* **2005**, *308*, 1607–1609.
(9) Liaw, J. W. *IEEE J. Sel. Top. Quantum Electron.* **2008**, *14*, 1441–1447.
(10) Fischer, H.; Martin, O. J. F. *Opt. Express* **2008**, *16*, 9144–9154.
(11) Sundaramurthy, A.; Schuck, P. J.; Conley, N. R.; Fromm, D. P.; Kino, G. S.; Moerner, W. E. *Nano Lett.* **2006**, *6*, 355–360.
(12) Merlein, J.; Kahl, M.; Zuschlag, A.; Sell, A.; Halm, A.; Boneberg, J.; Leiderer, P.; Leitenstorfer, A.; Bratschitsch, R. *Nat. Photonics* **2008**, *2*, 230–233.
(13) Chu, Y.; Schonbrun, E.; Yang, T.; Crozier, K. *Appl. Phys. Lett.* **2008**, *93*, 181108.
(14) Auguie, B.; Barnes, W. *Phys. Rev. Lett.* **2008**, *101*, 143902.
(15) Lesuffleur, A.; Kumar, L.; Gordon, R. *Phys. Rev. B* **2007**, *75*, No. 045423.
(16) Beversluis, M.; Bouhelier, A.; Novotny, L. *Phys. Rev. B* **2003**, *68*, 115433.
(17) Eftekhari, F.; Gordon, R. *IEEE J. Sel. Top. Quantum Electron.* **2008**, *14*, 1552–1558.
(18) Markel, V. *J. Phys. B* **2005**, *38*, L115–L121.
(19) Jureller, J.; Kim, H.; Scherer, N. *Opt. Express* **2006**, *14*, 3406–3414.
(20) McMahon, M.; Bowie, C.; Lopez, R.; Feldman, L.; Haglund, R., Jr. *Proc. SPIE* **2006**, *6106*, No. 61061N−1.
(21) Ferrara, D.; McMahon, M.; Lopez, R.; Haglund, R., Jr. *Proc. SPIE* **2007**, *6458*, No. 64581K1−11.
(22) Dadap, J.; Shan, J.; Heinz, T. *J. Opt. Soc. Am. B* **2004**, *21*, 1328–1347.
(23) Bouhelier, A.; Beversluis, M.; Hartschuh, A.; Novotny, L. *Phys. Rev. Lett.* **2003**, *90*, No. 013903.

DOI: 10.1021/nl102751m | *Nano Lett.* **2011,** *11,* 61–65